Journal of Hazardous Materials Advances 22 (2026) 101247

Contents lists available at ScienceDirect

Journal of Hazardous Materials Advances

journal homepage: www.elsevier.com/locate/hazadv

Toxicity and fate of silver nanoparticles from the food additive E174: Mitochondrial dynamics underlie their effects in intestinal epithelial cells

ND Saenen [a,*], S De Vos [a], E Verleysen [b], MS Witters [a], F Van Belleghem [a,c], J Mast [b], K Smeets [a]

[a] Zoology, Biodiversity and Toxicology, Centre for Environmental Sciences, Hasselt University, Diepenbeek, Belgium
[b] Service Trace Elements and Nanomaterials, Sciensano, Brussels, Belgium
[c] Department of Environmental Sciences, Open Universiteit, Heerlen, the Netherlands

ARTICLE INFO

Keywords:
Food additive
Scanning transmission electron microscopy
Oxidative stress
Caco-2
AgNPs

ABSTRACT

The safety of silver nanoparticles (AgNPs) in the food additive E174 is poorly understood. We conducted a comparative analysis of the toxicity profiles of AgNPs extracted from commercially available E 174-containing confectionery (E174-AgNPs) and polyvinylpyrrolidone-coated AgNPs (PVP-AgNPs) by studying redox- and mitochondrial stress responses in Caco-2 cells. Integrating biological findings with physicochemical characterisation and intracellular fate analysis revealed time- and concentration-dependent membrane damage for both AgNPs types. This was accompanied by an adaptive response to oxidative stress, as evidenced by gene expression changes of heme oxygenase 1 and other genes, and altered mitochondrial homeostasis and function, shown by changes in mitochondrial footprint and network morphology. Qualitative STEM-EDX after 24 h exposure indicated transformed E174-AgNPs in endo-/autolysosomes and silver-containing particles of a few nm in size near these structures in the cytoplasm, which culminated in mitochondrial swelling and rupture. The concurrent observation of an enhanced mitochondrial network morphology suggested a compensatory response by the remaining mitochondria. This comparative analysis of the toxicity of E174-AgNPs and PVP-AgNPs underscores the urgent need to reassess the safety of the food additive E 174. Our study highlights the importance of a comprehensive and in-depth evaluation of AgNP properties for accurate and robust hazard and risk assessments.

1. Introduction

Silver nanoparticles (AgNPs) are used in various applications, such as cosmetics, textiles, pharmaceuticals, household goods, and food packaging, because of their antimicrobial properties. Alongside these non-food applications, studies have confirmed the presence of AgNPs in the food additive E 174 (E174-AgNPs) (Verleysen et al., 2015; de la Calle et al., 2018), which are utilised to coat confectionery items (EFSA, 2025, 2016). These findings show that humans are exposed to E174-AgNPs. In its scientific opinion on the re-evaluation of E 174 as a food additive in 2016 and its follow-up in 2025, the European Food Safety Authority (EFSA) stated that there is insufficient data to assess the safety of the use of E 174 for its intended purpose (EFSA, 2025, 2016). Key knowledge gaps include uncertainties in particle size distribution, quantification of nanoparticles in food, kinetics of ionic silver (Ag^+) release, and insufficient characterisation of materials used in existing toxicity studies.

So far, the toxicity of AgNPs has mainly been studied for non-food-derived spherical NPs. *In vivo* biodistribution studies in rodents, conducted following various exposure routes, revealed accumulation of both AgNPs and newly formed secondary (transformed) Ag-containing nanoparticles in almost all organs - including the liver, kidney, spleen, brain, and heart - as detected by single-particle induced coupled mass spectrometry (Ferdous and Nemmar, 2020). This accumulation was associated with toxic effects such as inflammation, oxidative stress, DNA damage, and often resulted in cell death (Gan et al., 2020; Liao, Li, and Tjong, 2019). *In vitro* studies demonstrated that AgNPs enter human cells primarily via endocytic pathways (*e.g.*, pinocytosis and phagocytosis) or following membrane disruption. Dissolved Ag^+ ions may also cross membranes via passive diffusion or ion channels (Liao, Li, and Tjong, 2019; Panzarini et al., 2018), with similar toxicity effects to those observed *in vivo* studies (De Matteis, 2017). Evidence suggests that oxidative stress is a key mechanism through which AgNPs induce toxicity, either via the direct formation of reactive oxygen species (ROS) (Dąbrowska-Bouta et al., 2019) or by interacting with antioxidant defence mechanisms (AshaRani et al., 2009; Aueviriyavit, Phummiratch, and Maniratanachote, 2014; Song et al., 2014), by

* Correspondence author.
E-mail address: nelly.saenen@uhasselt.be (N. Saenen).

https://doi.org/10.1016/j.hazadv.2026.101247
Received 10 September 2025; Received in revised form 6 May 2026; Accepted 20 May 2026
Available online 22 May 2026

mitochondrial dysfunction (Bouwmeester et al., 2011; Maurer and Meyer, 2016; Miethling-Graff et al., 2014), or by inducing inflammatory processes (Martirosyan et al., 2016), or damage to cellular components (DNA, functional lipids or proteins, cell membrane) (De Matteis, 2017; Akter et al., 2018). Studies suggest that the toxicity may be caused by Ag^{+} released from the particles (Bouwmeester et al., 2011; Medina-Reyes et al., 2020). Hence, it is proposed that AgNPs are susceptible to transformations that may alter their ionic release and, consequently, their toxicity profile (Marchioni et al., 2018). Therefore, proper physicochemical characterisation of the AgNPs is crucial for evaluating toxicity related to their coating, structure, size, proportion of released ions, and even the specific intracellular area in which the AgNPs are localised (Bouwmeester et al., 2011; Molleman and Hiemstra, 2015; Polet et al., 2020).

Despite the general assumption that physicochemical properties are correlated with nanoparticle toxicity, many studies lack detailed and comprehensive characterisation data of the nanoforms under investigation, especially within a biological environment. This information is needed to address knowledge gaps and questions regarding food- and environment-specific nanoforms. Since food-related nanoforms, such as E174-AgNPs, enter the human body through food consumption, the gastrointestinal system is the main route of exposure. Therefore, hazard assessment of AgNPs in the gut is crucial for future risk assessment (Akter et al., 2018). To reduce the number of experimental animals for toxicity testing in compliance with the REACH regulation of the 3R principle - Replacement, Reduction and Refinement (Directive 2010/63/European Parliament), alternative models, such as *in vitro* gut models, are being proposed. Caco-2 cells are a human colon adenocarcinoma cell line with small intestine enterocyte-like properties (García-Rodríguez et al., 2018; Powell et al., 2010). Due to these properties, Caco-2 cells are widely used to investigate bioprocesses induced by nanoparticles in the intestine, either alone or in coculture with other cell types of the human intestinal epithelium.

This study contributes to addressing critical knowledge gaps concerning the safety of E174-derived silver nanoparticles by investigating whether well-established toxicological mechanisms for non-food AgNPs also apply to food-derived counterparts. Specifically, we conducted a comparative toxicity profiling of E174-AgNPs against well-characterised polyvinylpyrrolidone-coated AgNPs (PVP-AgNPs), focusing on redox signatures and mitochondrial function, and integrated these findings with a comprehensive characterisation of the physicochemical transformations and intracellular fate of E174-AgNPs upon uptake in Caco-2 cells. We hypothesise that the physicochemical transformations of E174-AgNPs after cellular uptake modulate redox processes and mitochondrial function, thereby triggering cytotoxic responses. Using an *in vitro* gut model, this study provides the first toxicity assessment of AgNPs derived from the food additive E 174 in external confectionery coatings, integrating both their physicochemical properties and biological effects. This dual approach both verifies known toxicological mechanisms in the context of food-related AgNPs and generates essential data for hazard assessment.

2. Methods

2.1. Selection of materials

Unless otherwise stated, all consumables, *in vitro* assays, stains, and equipment were purchased from Fisher Scientific (Brussels, Belgium). For specific experiments, commercially available spherical PVP-AgNPs (~0.2 wt%) (US Research Nanomaterials Inc., Houston, USA) were used. PVP-AgNPs are widely studied and well-characterised silver nanomaterials, with several toxicological mechanisms described in the literature. Their use therefore provides a robust benchmark for evaluating whether the biological effects of E174-AgNPs align with known toxicological mechanisms for non-food AgNPs. The stock suspension of PVP-AgNPs (1 mg/mL) in autoclaved sterile-filtered (0.2 µm PES) ultrapure water (18.2 MΩ•cm) (further referred to as Milli-Q) was freshly prepared before each experiment using the following protocol, repeated five times: sonication in a water bath (Ultrasonic Cleaner USC-TH, VWR, Belgium) at 45 Hz for 5 min, followed by vortex mixing for 30 s. The suspension was kept in a glass beaker surrounded by icy water to prevent overheating during the process. Exposure concentrations equivalent to those of the E174-AgNPs (128.7 µg/mL and 32.2 µg/mL) were prepared in serum-free cell culture medium (Sigma-Aldrich, Darmstadt, Germany).

2.2. Extraction of E174-AgNPs

A 3.3 g sample of the E 174-containing confectionery product Ag-P-009 (~20–22 product units), as described in more detail by De Vos et al., 2020, (2020), with a total silver content of 4.3 g/kg food product, was gradually added to 1 mL of Milli-Q water while stirring constantly. When the outer E174-containing coating was detached, the remaining sugar core of each silver sugar pearl was removed from the dispersion. This resulted in a silvery dispersion with a concentration of approximately 14.2 mg/ml total silver, with 0.4 ± 0.15 mass percentage accounted for the present nanoparticle fraction, as determined by single particle ICP-MS, and with the assumption that the total mass of silver of the food additive was equal to 1000 g/kg (De Vos et al., 2020). The remaining dispersion was transferred to 1.5 mL tubes (1 mL/tube). The samples were vortexed for 10 s and centrifuged for 11 h at 21,130 x g at room temperature. The supernatant was removed to wash away possible remaining food matrix components, and the pellets were resuspended in 100 µL Milli-Q to concentrate the sample. The samples were homogenised and transferred to a single 1.5 mL tube and centrifuged at 845 x g for 25 min to remove residual coarse food matrix components and large E174 flakes. The resulting supernatant containing the E174-AgNPs was recovered, gamma-irradiated at 30 Gy for 20 min using an IBL 437 C gamma steriliser (CIS bio international, Saclay, France), and used immediately for experiments. Exposure concentrations of 128.7 µg/mL (4.36-fold dilution of supernatant) and 32.2 µg/mL (17.4-fold dilution of supernatant) of the gamma-irradiated stock dispersion of E174-AgNPs were prepared in serum-free cell culture medium (Sigma-Aldrich, Darmstadt, Germany). These final exposure concentrations, corresponding to 9.7 and 38.6 µg E174AgNPs per cell culture well, and equivalent to ~12 and 48 E 174-containing confectionery product units, were calculated based on the total AgNP mass content of Ag-P-009 product quantified by single-particle ICP-MS, as described in De Vos et al., (2020). The *in vitro* exposure concentrations were primarily selected to enable effect-based toxicity assessment and comparison with existing literature of non-food AgNPs in different cell types, ranging from limited to severe toxicity (Wang et al., 2017; Xu, Basu, and George, 2021); therefore, the results should be interpreted in light of these concentrations, which may exceed typical real-world dietary exposure. For each experiment, the dispersion of E174-AgNPs was freshly prepared.

2.3. Physicochemical characterisation of E174-AgNPs and PVP-AgNPs

Physicochemical characterisation of E174-AgNPs and PVP-AgNPs was carried out with high-angle annular dark field (HAADF) scanning transmission electron microscopy (STEM) imaging and energy-dispersive X-ray spectroscopy (EDX) analysis at 200 kV by a Talos F200S G2 transmission electron microscope equipped with HAADF detector and a Super-X EDS detector (Thermo Fisher Scientific, Eindhoven, The Netherlands), using Velox software (Thermo Fisher Scientific). For quantitative particle size and shape measurements, at least 100 particles from 10 representative micrographs were analysed using the ParticleSizer software (Verleysen et al., 2019; Wagner, 2017).

To evaluate potential transformations of E174-AgNPs and PVP-AgNPs in cell culture medium compared with MilliQ water, particle size, morphology, and chemical composition were evaluated by STEM-

EDX. Zeta potential and hydrodynamic diameter were measured by dynamic light scattering (DLS) (Zetasizer Ultra, Malvern Panalytical, Netherlands). STEM-EDX results were presented as minimum Feret diameter (Feret min), maximum Feret diameter (Feret max), aspect ratio, and solidity. DLS results were reported as the Z-average hydrodynamic diameter (intensity-weighted mean size), Zeta-potential, Polydispersity Index (PI), and the relative intensity-weighted mean diameter of the first size-distribution peak.

2.4. Cell culture and experimental settings

Adherent human epithelial colorectal adenocarcinoma cells (Caco-2, ATCC® HTB-37™, LGC Standards, Wesel, Germany) were cultured and maintained in 75 cm^2 cell culture flasks (Greiner, Sigma-Aldrich, Darmstadt, Germany) containing Dulbecco's Modified Eagle Medium (DMEM) supplemented with 10% (v/v) heat-inactivated foetal bovine serum (FBS) (Sigma-Aldrich, Darmstadt, Germany), 1% (v/v) Penicillin/Streptomycin (P/S) and 1% (v/v) Non-Essential Amino Acids (MEM-NEAA). Cells were cultivated at 37 °C and 5% CO_2, and the medium was refreshed every 2–3 days. Subculturing was carried out at 50–70% confluence. For each experiment, cells were seeded at 1.5×10^4 cells/cm^2, unless stated otherwise. Caco-2 cells of passages 30–40 were grown for 4–5 days to reach a confluent Caco-2 monolayer (non-synchronised cells). The selected exposure concentrations were applied in 24-well plates for 5 h and 24 h, respectively, in 300 μL DMEM medium without FBS, unless stated otherwise. These exposure times were chosen to capture both early and late cellular responses to AgNPs, as previously described in literature (Chen et al., 2016; Bouwmeester et al., 2011 and 2016, Aueviryavit S et al., 2014).

2.5. Cell viability, redox, and mitochondrial measurements

2.5.1. Cell viability assays

Cell viability of Caco-2 cells was determined after 5 h and 24 h exposure to E174-AgNPs and PVP-AgNPs. Membrane damage was measured using the CyQuant LDH cytotoxicity assay following the manufacturer's protocol. The optical density of viable cells (absorbance at 490 nm and 680 nm) was determined using a microplate reader (Fluostar Omega, BMG Labtech, Champigny-sur-Marne, France). Results were expressed as % membrane damage, normalised for spontaneous LDH release from untreated cells and maximum LDH release following complete cell lysis. A positive assay control from the assay kit was included. Interference of the E174-AgNPs and PVP-AgNPs with the readout signal of the LDH assay was evaluated and did not affect the results (Supplemental Figure A1). Metabolic activity, quantified with the MTT cell proliferation assay (ATCC® 30–1010 K, LGC Standards, Wesel, Germany), was used for confirmation purposes and measured only after 24 h exposure to E174-AgNPs. Absorbance was measured at 570 nm. Results were expressed as metabolic activity relative to the respective control.

2.5.2. Transcriptional analysis with RT-qPCR

Gene expression of redox-related genes was assessed after 5 h and 24 h exposure to E174-AgNPs and PVP-AgNPs. Briefly, Caco-2 cells were harvested and immediately stored at −80 °C. Total RNA was isolated by means of phenol-chloroform extraction and stored at −80 °C for up to 3 months. The total RNA concentration and sample purity were determined using a NanoDrop spectrophotometer (ND-1000, Fisher Scientific, Belgium). Total RNA was DNase-treated with the Turbo DNA-free kit and then reverse-transcribed to cDNA using Superscript III First-Strand Synthesis Supermix. cDNA was stored at −20 °C until further use. qPCR primers were developed with NCBI primer blast. Primer efficiency and non-specific targeting were assessed using RT-qPCR (Applied Biosystems Quantstudio 5 qPCR system). For selection of genes and primer information, see Supplementary Table A1. Gene expression was analysed on a 384-well plate using a PCR mix containing 5 μL FAST SYBR green, 0.3 mM of each primer, 1.9 μL nuclease-free water, and 2.5 μL cDNA template (10 ng/μL). Cycling conditions consisted of an initial denaturation at 95 °C for 20 s, followed by 40 cycles of 95 °C for 1 s and 60 °C for 20 s. Raw data were processed using QuantStudio Design & Analysis software to obtain Ct values. The $2^{-\Delta\Delta Ct}$ method, normalised for three reference genes (Supplementary Table A1), was applied to calculate the gene expression relative to the control. Reference genes were selected based on the geNorm algorithm in the qBasePLUS version 2.0 software (Biogazelle, Ghent, Belgium). Gene expression analysis was performed in two independent experiments with six biological replicates, and MIQE guidelines were considered (Bustin et al., 2009).

2.5.3. Hydrogen peroxide assay

To complement transcriptional analyses, hydrogen peroxide levels were quantified after 24 h exposure of the Caco-2 cells to E174-AgNPs. Cells were washed twice with PBS (-Ca^{2+}, -Mg^{2+}), trypsinised, resuspended in DMEM medium with FBS, and centrifuged at 300 x g for 5 min. The resulting pellet was resuspended in 70 μL of 1x assay buffer from the Oxiselect™ Hydrogen Peroxide/Peroxidase Assay Kit (Cell Biolabs, Bio-connect, Huissen, the Netherlands), and 3–5 glass beads were added for mechanical disruption using a Retsch mixer mill MM400 (1 min at 30 Hz). Hydrogen peroxide levels were then determined from 50 μL of the sample following the kit protocol. Fluorescence intensity was measured at 544–10 nm excitation and 590–10 nm emission with a Fluostar Omega microplate reader (BMG Labtech, Champigny-sur-Marne, France). To account for differences in cell mass, H_2O_2 levels were normalised to total protein content, quantified using the Bio-Rad protein assay (Bio-Rad Laboratories, Temse, Belgium) according to the manufacturer's instructions.

2.5.4. Mitochondrial network morphology imaging

After treatment with E174-AgNPs and PVP-AgNPs for 5 h and 24 h in 8-well IBIDI chambers (Ibidi GmbH, Gräfelfing, Germany), Caco-2 cells were stained with 250 nM Mitotracker Red CMXRos (dark, 37 °C, 5% CO_2) and imaged on a Zeiss LSM900 confocal laser scanning microscope (Zaventem, Belgium) at 40x magnification, using Ex/Em: 579/599 nm. Five tile scans per treatment were acquired, and mitochondrial morphology was analysed using ImageJ 2.90/1.53t (NanoDefine 2016) and the MiNA tool (Valente et al., 2017). For each image, 5–10 cells were randomly selected to quantify mitochondrial footprint, branch length, and network branches. Detailed procedures are provided in Supplementary Methods.

2.5.5. Mitochondrial DNA content

To confirm the mitochondrial footprint findings, mitochondrial DNA content (mtDNAc) was measured after 24 h exposure to 32.2 μg/mL and 128.7 μg/mL E174-AgNPs as previously described (Saenen et al., 2023). Primer sequences are provided in Supplementary Methods.

2.5.6. Statistical analysis

Unless otherwise stated, cellular and molecular assays were performed in triplicate across two independent experiments. Statistical analyses were performed using JMP® Pro 16 (JMP Benelux, Medhenham Marlow, UK). Data normality and homogeneity of variances were assessed using the Shapiro-Wilk test and Bartlett's test, respectively. Parametric data were analysed by one-way analysis of variance (ANOVA) followed by Tukey post hoc test, whereas nonparametric data were evaluated using the Steel-Dwass or Dunn's multiple comparison tests after unsuccessful data transformation. Results are presented as mean ± standard deviation (SD) or standard error to the mean (SEM) relative to the control, with $p\text{-value} < 0.05$ considered statistically significant.

2.6. E174-AgNPs uptake and effects on cellular ultrastructure

Caco-2 cells were grown on Nunc™ Thermanox™ coverslips (13 mm

diameter) in a 24-well plate. When a confluent monolayer was reached, cells were exposed to 128 μg/mL E174-AgNPs for 24 h in 300 μL cell culture medium without FBS. The cells were then washed with PBS and fixed for 2 h in 1 mL 2% glutaraldehyde in 0.05 M Na-cacodylate buffer (pH 7.3). After fixation, cells were stored in 1 mL 0.05 M Na-cacodylate buffer (pH 7.3) containing 0.15 M saccharose (295 mOsm) at 4 °C. Multiple dehydration steps in acetone, followed by embedding in Embed 812 (Electron Microscopy Sciences, Hatfield, PA, USA), were used to prepare resin-embedded cells. Ultrathin sections of 80 nm, 100 nm, 120 nm, or 150 nm thick of these cells were cut and collected on carbon- and pioloform-coated 150 or 400 mesh grids (Agar Scientific, Stansted, UK) using an ultramicrotome. Intracellular E174-AgNPs uptake was examined with HAADF-STEM-EDX using the same settings described previously. TEM imaging was performed to assess the effects on cellular ultrastructure using a Tecnai G2 Spirit TEM with BioTwin lens configuration (Thermo Fisher Scientific, Eindhoven, The Netherlands), equipped with a bottom-mounted 4 × 4 K Eagle CCD-camera.

3. Results

To evaluate the comparative toxicity profile of E174-AgNPs and PVP-AgNPs, we employed a well-established Caco-2 *in vitro* model of the human intestinal epithelium. Concentration ranges were chosen to reflect literature-reported dose-dependent effects of non-food AgNPs,

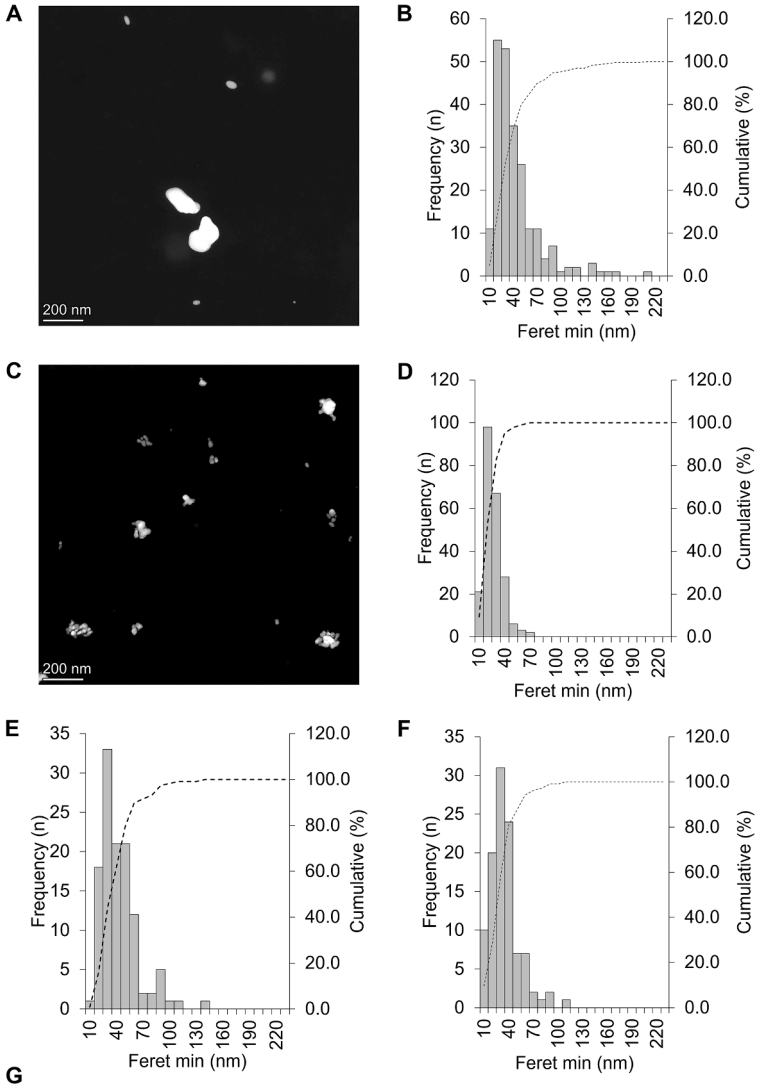

G

Condition	Feret min (nm) mean ± SD	Feret max (nm) mean ± SD	Aspect ratio mean ± SD	Solidity mean ± SD
E174 AgNP stock 1	38 ± 21	56 ± 37	1.46 ± 0.37	1.00 ± 0.004
E174 AgNP stock 2	37 ± 30	60 ± 63	1.43 ± 0.45	0.97 ± 0.05
E174 AgNP in culture medium	29 ± 18	42 ± 30	1.34 ± 0.32	0.97 ± 0.04
PVP AgNP stock	23 ± 12	31 ± 16	1.38 ± 0.30	0.99 ± 0.002

Fig. 1. Size distribution of the E174-AgNPs and PVP-AgNPs. Selected HAADF image of E174-AgNPs in Milli-Q (**A**) and PVP-AgNPs in Milli-Q (**C**) (scale bar = 200 nm, image size = 2048 px x 2048 px, image resolution 0.8 nm/px). Histograms of the size distribution of the E174-derived AgNP stock 1 recovered after centrifugation and gamma treatment in Milli-Q (**B**), PVP-AgNP stock after 30 min sonication in a water bath (**D**), the E174-derived AgNP stock 2 recovered after centrifugation and gamma treatment in Milli-Q (**E**), and the E174-derived AgNP stock 2 dispersed in DMEM culture medium without FBS (**F**). Mean ± SD of the minimum and maximum Feret diameter in nm, aspect ratio, and solidity for the E174-derived AgNP and PVP-AgNP stocks, and the E174-derived AgNP in culture medium (**G**).

spanning from mild to severe toxicity in different cell types. This approach enabled assessment of the potential hazard of E174-AgNPs while facilitating direct comparison with existing knowledge on coated AgNPs. Given the established role of oxidative and mitochondrial stress in non-food AgNPs cytotoxicity, we specifically analysed these stress responses for both particle types. Following this comparative screening, we then performed a more detailed and in-depth qualitative characterisation of the localisation of E174-AgNPs in Caco-2 cells and their accompanying ultrastructural changes using HAADF-STEM-EDX and TEM, respectively.

3.1. Physicochemical properties of E174-AgNPs

Figs. 1 and 2 summarise the properties of the E174-AgNPs and PVP-AgNPs dispersed in Milli-Q or cell culture medium, as characterised by STEM-EDX and DLS, respectively. The size of dispersed E174-AgNPs was similar across stock suspensions in Milli-Q but smaller in cell culture medium, with mean Min Feret diameters of 38 nm (stock 1), 37 nm (stock 2), and 29 nm (medium) (Fig. 1B; E-F), with an expanded uncertainty (95%, k = 2) of 15.1% for triplicate analysis and 18% for single measurements. The mean Feret min of PVP-AgNPs was 23 nm (Fig. 1D). The morphology of both the E174-AgNPs and PVP-AgNPs showed spheroidal particles (Fig. 1A; C), as defined in the Appendix for nanoforms applicable to the guidance on registration and substance identification (European Chemical Agency ECHA, 2022), with spherical to oval shape, as represented by the mean aspect ratios of 1.46 and 1.38 in Milli-Q, respectively.

DLS measurements (Fig. 2) showed larger apparent particle sizes compared with STEM-EDX, as expected for hydrodynamic diameters. In stock suspensions, the Z-average hydrodynamic diameter was 158.9 ± 11.1 nm for E174-AgNPs and 164.6 ± 4.5 nm for PVP-AgNPs, with intensity-weighted peak diameters of 180.1 ± 3.5 nm and 209.2 ± 15.1 nm, respectively (Fig. 2C). The zeta potential of the PVP-AgNP stock suspension was −32.5 mV, indicating good colloidal stability, whereas E174-AgNPs showed a lower surface charge (−7.59 mV).

Upon dispersion in cell culture medium, both materials exhibited an increase in hydrodynamic diameter over time, consistent with agglomeration processes. For E174-AgNPs, the Z-average increased from 196.5 ± 8.5 nm at 0 h to 575.8 ± 23.7 nm after 5 h and further to 2540 ± 198.1 nm after 24 h, with corresponding peak one intensity diameters shifting from 154.7 ± 2.8 nm to 551.9 ± 58.3 nm and 1205 ± 378.6 nm (Fig. 2A, C). PVP-AgNPs showed a similar but less pronounced trend, with the Z-average increasing from 335.1 ± 15.4 nm at 0 h to 1164 ± 63.8 nm after 5 h and 887.4 ± 290.2 nm after 24 h, and peak one intensity diameters of 247.5 ± 16.3 nm, 482.5 ± 31.7 nm, and 493 ± 137.9 nm, respectively (Fig. 2B, C). Overall, while both AgNPs displayed comparable hydrodynamic sizes in stock suspensions, time-dependent agglomeration in culture medium was more pronounced for the E174-AgNPs.

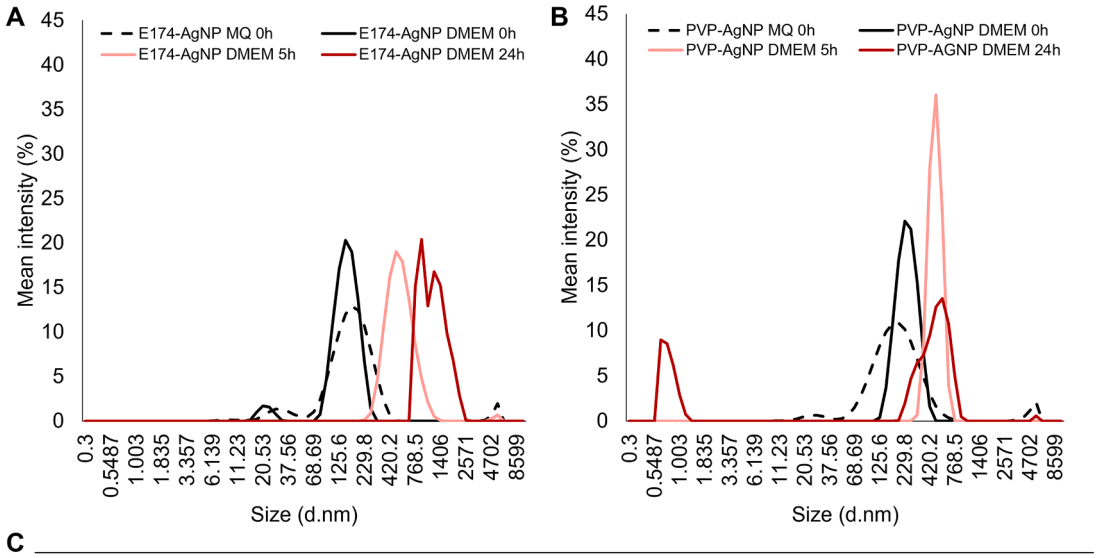

C

Condition	Time (h)	Zeta Potential (mV)	Z-average (nm)	PI	Peak One mean by intensity (nm)
			mean ± SD		
E174 AgNP stock	0	-7.59	158.9 ± 11.1	0.42 ± 0.05	180.1 ± 3.5
E174 AgNP in culture medium	0	/	196. 5 ± 8.5	0.29 ± 0.03	154.7 ± 2.8
	5		575.8 ± 23.7	0.36 ± 0.05	551.9 ± 58.31
	24		2540 ± 198.1	0.64 ± 0.18	1205 ± 378.6
PVP AgNP stock		-32.5	164.6 ± 4.5	0.43 ± 0.04	209.2 ± 15.1
PVP AgNP in culture medium	0	/	335.1 ± 15.4	0.40 ± 0.02	247.5 ± 16.3
	5		1164 ± 63.8	0.66 ± 0.04	482.5 ± 31.7
	24		887.4 ± 290.2	0.62 ± 0.11	493 ± 137.9

Fig. 2. Characterisation of AgNP dispersions and their temporal evolution in cell culture medium. (**A**) Intensity-weighted size distributions of E174-AgNPs measured by DLS after dispersion in Milli-Q (MQ) water (0 h) and in DMEM cell culture medium at 0, 5, and 24 h. (**B**) Intensity-weighted size distributions of PVP-AgNPs under the same conditions. Curves illustrate time-dependent changes in hydrodynamic size following dispersion in cell culture medium. (**C**) Summary of DLS-derived parameters for both AgNPs, including zeta potential (mV), Z-average hydrodynamic diameter (nm), polydispersity index (PI), and peak one mean diameter by intensity. Values are reported as mean ± SD.

3.2. Cytotoxicity and redox changes induced by E174-AgNPs and PVP-AgNPs

A concentration-dependent cytotoxicity effect was observed for both E174-AgNPs (128.7 μg/mL: 34.9 ± 9.6%, p = 0.002) and PVP-AgNPs (128.7 μg/mL: 27.8 ± 14.5%, p < 0.001) after 24 h exposure, while no cytotoxicity was visible after a 5 h exposure duration (Fig. 3A). The induced cytotoxicity was confirmed by a decreased metabolic activity of 43.4% (± 3.5%, p < 0.0001) after 24 h exposure to 128.7 μg/mL E174-AgNPs (Supplemental figure A2).

The expression patterns of several redox-related genes were significantly altered for both E174-AgNPs and PVP-AgNPs in a time- and concentration-dependent manner (Fig. 3B). Heme oxygenase-1 (*HMOX-1*) was differentially expressed (Fold change > 1.5, p < 0.05) in all exposure conditions compared to the controls. NADPH oxidase 1 (*NOX1*) was significantly upregulated after 24 h exposure for both E174-derived and PVP-AgNPs, and specifically at the highest exposure concentration (Fold change > 2, p < 0.01). No changes were found in the expression of the transcription factor nuclear factor erythroid-derived 2 related factor 2 (*NRF2*) and the tumour protein P53 (*TP53*). Genes involved in antioxidant defence cascades, such as catalase 1 (*CAT1*) and glutathione peroxidase 1 (*GPX1*), were downregulated when exposed for 24 h to the highest exposure concentration of both E174-AgNPs and PVP-AgNPs (Fold change < 0.5, p < 0.05). However, the expression patterns of glutathione S transferase pi 1 (*GSTP1*) and superoxide dismutase (*SOD1* and *SOD2*) genes were not significantly altered. Several metal-transporter genes, including the Antioxidant 1 Copper Chaperone (*ATOX1*) gene, which encodes Cu-chaperones in enterocytes, and Divalent metal transporter 1 (*DMT1* or *SLC11A2*), involved in cellular copper homeostasis, were reduced in expression (Fold change < 0.5; p < 0.001) after 24 h exposure, especially for the E174-AgNPs. The transporters high-affinity copper uptake protein 1 (*CTR1* or *SLC31A1*) and heme carrier protein 1 (*HCP1* or *SLC46A1*) showed no expression changes compared to the control treatment. To further unravel the specificities of the altered redox signature, H_2O_2 was measured after 24 h exposure to the E174-AgNPs. All exposed cells reduced H_2O_2 levels, with a significant reduction for the highest exposure (128.7 μg/mL: 47.6% ± 8.9%, p = 0.009 compared to control) (Supplemental Figure A3, panel A).

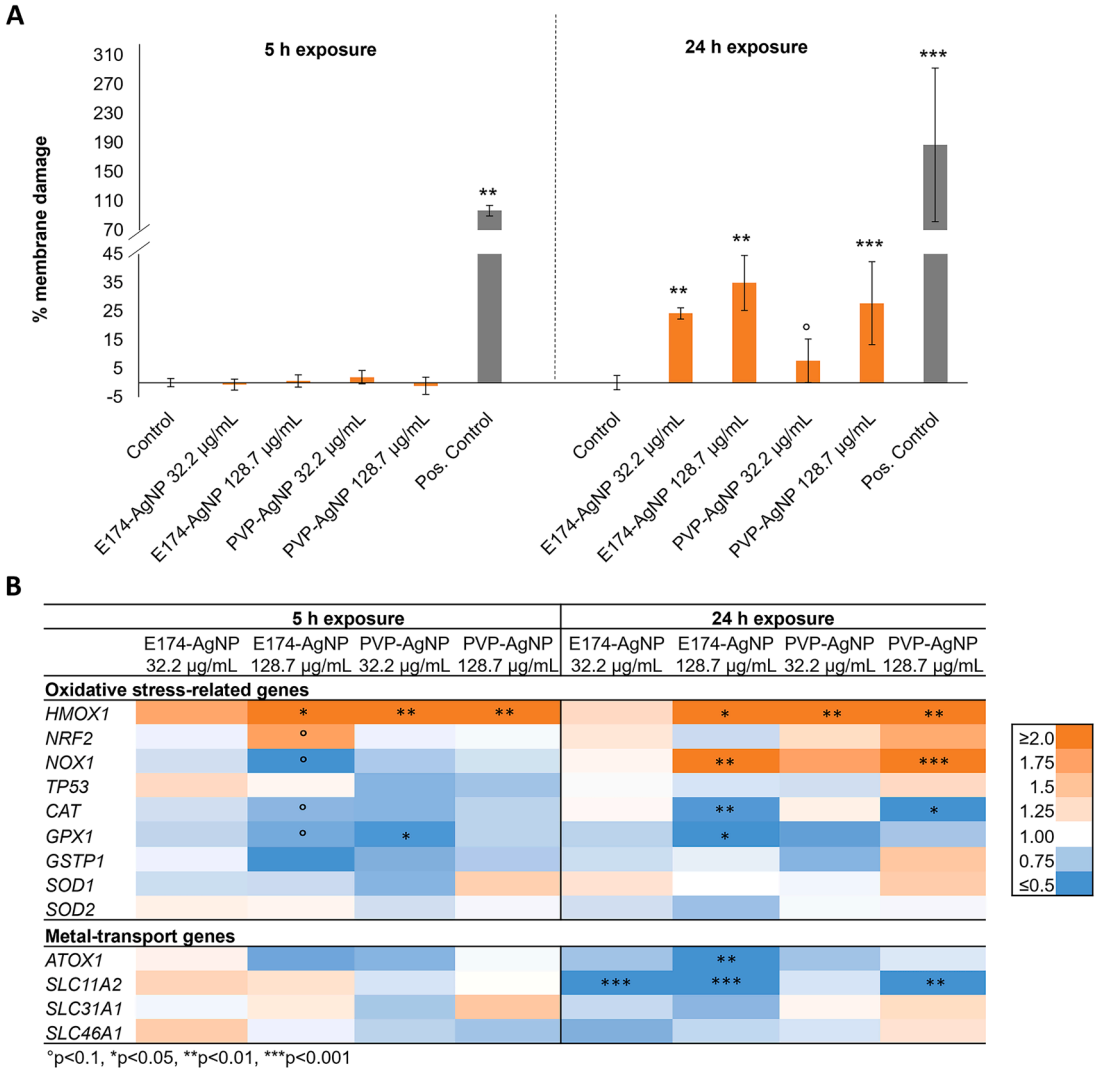

Fig. 3. Cytotoxicity and gene-expression changes of E174-AgNPs and PVP-AgNPs in a Caco-2 monolayer. (**A**) Cytotoxicity was assessed with the LDH assay and presented as percentage membrane damage ± SD (N = 6–20 from at least two independent experiments). Statistical significance was tested using a nonparametric comparison with the Dunn method. ° p < 0.1, *p < 0.05, ** p < 0.01, *** p < 0.001. (**B**) Gene expression was assessed with qPCR and the ΔΔCt method and presented as the fold change difference compared to control (N = 12 from two independent experiments). Statistical significance was tested using a nonparametric comparison with the Dunn method. ° p < 0.1, *p < 0.05, ** p < 0.01, *** p < 0.001.

3.3. Effects of E174-AgNPs and PVP-AgNPs on mitochondrial footprint and network morphology

The mitochondrial footprint and network morphology were determined with the aid of live-cell confocal microscopy using the Mitotracker CMXRos stain, revealing significantly increased mitochondrial footprints after 5 h exposure to PVP-AgNPs (% to control ± SEM: 27.0% ± 7.8%, p = 0.0054 for 32.2 μg/mL PVP-AgNPs; 24.6% ± 6.5%, p = 0.0078 for 128.7 μg/mL PVP-AgNPs). No significant differences were observed for the E174-AgNPs at this time point (Fig. 4A). A longer exposure (24 h) resulted in reduced mitochondrial footprints after exposure to the E174-AgNPs (% to control ± SEM: −25.8% ± 2.9%, p <

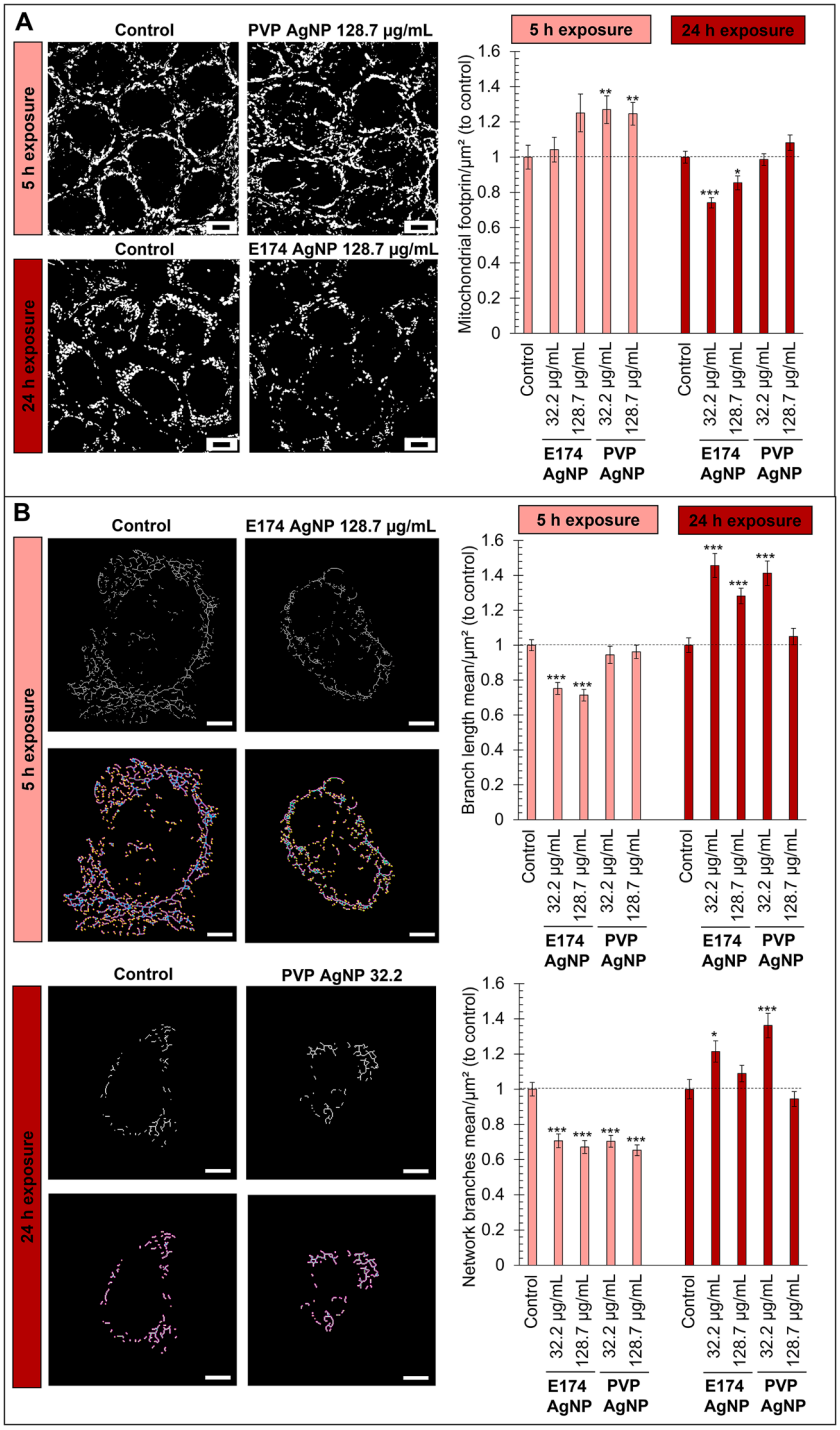

Fig. 4. Mitochondrial morphology analysis after 5 h and 24 h exposure to E174-AgNPs and PVP-AgNPs. Selected binary images depicting the active mitochondria after 5 h and 24 h exposure to E174-AgNPs and PVP-AgNPs compared to their respective controls (Scale bar = 5 μm) (panel **A**). The Mitochondria Network Analysis tool (MiNA) on the ImageJ interface was used for quantitative assessment of the mitochondrial footprint/μm² relative to control, of which results are shown in panel A (n = 86–106 cells/treatment from two independent experiments). Selected skeletonised images of the mitochondrial network structure after 5 h and 24 h exposure to E174-AgNPs and PVP-AgNPs compared to their respective control (Scale bar = 5 μm) (panel **B**). Quantitative assessment by the MINA tool of the branch length/μm² and network branches/μm² is shown in panel B (n = 86–106 cells/treatment from two independent experiments). Statistical significance was tested with a nonparametric comparison using the Steel-Dwass method (*p < 0.05, **p < 0.01, ***p < 0.001).

0.0001 for 32.2 μg/mL; −14.6% ± 3.9%, p = 0.01 for 128.7 μg/mL), but not to the PVP-AgNPs (Fig. 4A). The concentration-dependent decrease in mtDNAc after 24 h exposure to E174-AgNPs further complemented these findings (Supplemental Figure A3, panel B).

Mitochondrial morphology, including branch length and number of network branches, showed opposing trends between the two exposure durations. Overall, a decrease in branch length (% to control ± SEM: −24.8% ± 3.4%, p < 0.0001 for 32.2 μg/mL; −28.6% ± 3.4%, p < 0.0001 for 128.7 μg/mL) and network branches (% to control ± SEM: −29.3% ± 4.0%, p < 0.0001 for 32.2 μg/mL; −32.8% ± 3.6%, p < 0.0001 for 128.7 μg/mL) was found after 5 h exposure to E174-AgNPs, whereas for PVP-AgNPs only a difference was observed in the number of network branches (% to control ± SEM: −29.5% ± 3.4%, p < 0.0001 for 32.2 μg/mL; −34.7% ± 3.0%, p < 0.0001 for 128.7 μg/mL). A 24 h exposure resulted in an increase in branch length means for both E174-AgNPs (% to control ± SEM: +45.7% ± 6.9%, p < 0.0001 for 32.2 μg/mL; +28.2% ± 4.4%, p < 0.0001 for 128.7 μg/mL) and PVP-AgNPs (% to control ± SEM: +41.3% ± 7.0%, p = 0.0001 for 32.2 μg/mL) (Fig. 4B). An increase in network branches was only observed at the lowest exposure concentration (% to control ± SEM: +21.4% ± 6.1%, p = 0.017 for E174-AgNPs; +36.2% ± 6.9%, p = 0.0005 for PVP-AgNPs).

3.4. Analysis of E174-AgNPs uptake, transformation, and intracellular damage

Because toxicity responses were mainly observed after 24 h exposure, uptake, transformation, and intracellular damage of E174-AgNPs were imaged and analysed by HAADF-STEM-EDX in ultra-thin sections of Caco-2 cells at this time point. The majority of E174-AgNPs were sequestered in cellular vesicles resembling endo-/autolysosomes with intraluminal vesicles (Figs. 5A–C, Supplemental Figures A4 and A6), yet silver-containing particles of a few nm were observed inside the cytoplasm, near the vesicles (Fig. 5C–D). The EDX spectra and the elemental maps of the nano-structures showed that the observed particles in Caco-2 cells are E174-derived Ag-containing particles (Figs. 5E–F, Supplemental Figure A5). Some particles analysed by EDX only displayed an Ag X-ray signal (Fig. 5, Supplemental Figure A5), while other particles displayed co-localisation of Ag with a low sulphur X-ray signal (Supplemental Figure A6).

As shown in the micrographs of Fig. 6, exposure of Caco-2 cells to E174-AgNPs caused swelling and rupture of the mitochondria, as well as damage to the cristae. Furthermore, the mitochondria of the exposed cells appeared to show more electron-dense precipitates (Figs. 6B–D) compared to the control cells (Figs. 6A–C), suggesting the formation of $Ca_3(PO4)_2$, a well-known phenomenon in mitochondria under stress. Compared to the control cells, electron-lucent cytoplasm was observed (Figs. 6B–D), indicating degeneration caused by oxidative stress. Additionally, the cytoplasm displayed vacuolation, as indicated by the abundance of vesicles (Figs. 6B–D) and endo-/autolysosomes (Figs. 6B–C). STEM analysis showed that a limited number of the endo-/autolysosomes had sequestered E174-AgNPs (Fig. 5).

4. Discussion

To our knowledge, this is the first comprehensive study investigating well-known toxicological mechanisms associated with non-food AgNPs to verify the hazards of the nanoscale fraction of the food additive E 174 (E174-AgNPs) in the gut. For comparison with existing data in the literature, a non-food silver nanoparticle (PVP-AgNPs) was included in the general cytotoxicity and mechanism-of-action analyses. The study's strength lies in (i) the use of AgNPs extracted directly from confectionery products (E174), (ii) their comparative toxicological and mechanistic profiling against well-characterised PVP-coated AgNPs across two exposure durations (5 h and 24 h), and (iii) the integration of these findings with a detailed physicochemical characterisation of E174-AgNPs before and after cellular uptake, linking observed toxicity to ultrastructural localisation and nanoparticle transformations. This methodological framework aligns with requirements outlined in several EFSA reports (EFSA 2025) and provides pivotal information for hazard identification and future risk assessment of the food additive E174 (Brandon et al., 2006; Gerloff et al., 2009; Lefebvre et al., 2015).

This study aimed to integrate particle characteristics and induced cellular toxicity for proper hazard characterisation of E174-AgNPs, with HAADF-STEM-EDX providing ultrastructural insight. The spheroidal E174-derived nanoparticles were engulfed in endo-/autolysosomes of the Caco-2 cells, demonstrating particle uptake through the endocytic route. Both individual particles and loosely agglomerated forms were identified in the vesicles, in line with *in vitro* studies using non-food AgNPs reporting particles in multivesicular bodies (Persaud et al., 2019), late endosomes (Wu et al., 2019), endolysosomes (Zhang, Shen, and Gurunathan, 2016), lysosomes (van der Zande et al., 2016; Taboada-López et al., 2021), and autophagosomes (Taboada-López et al., 2021; Porter et al., 2021). In addition, several smaller E174-derived silver-containing entities were observed in the cytoplasm adjacent to endo-/autolysosomes. These "particles", defined by visible physical boundaries in the electron micrographs (ISO26824:2022 2022) in the cytoplasm near the endo-/autolysosomes, have also been observed in non-food AgNPs (Wu et al., 2019; Lichtenstein et al., 2017a), and may represent either residual fragments of disintegrated AgNPs or Ag^+ ions that reprecipitated following lysosomal solubilisation (Zhang, Shen, and Gurunathan, 2016). This interpretation aligns with reported size reductions of AgNPs post-uptake (van der Zande et al., 2016; Bobyk et al., 2021), which are often facilitated by Ag^+ ion release under acidic lysosomal conditions (Loza et al., 2014).

Both AgNPs and Ag^+ ions have a high affinity for sulphur species, consistent with our qualitative observation of vesicular AgNPs colocalising with a sulfur X-ray signal. Similar transformations have been reported for non-food AgNPs (Marchioni et al., 2018), where intracellular Ag_2S formation is linked to binding with S-rich thiols, such as glutathione, chaperones, and detoxifying enzymes, including metallothioneins (Ferreira et al., 2020; Liu et al., 2012). The consequences of sulphur interactions are complex: although sulfidation of Ag-NPs (Ag_2S-NPs) in most cases causes a marked reduction in toxicity due to the extremely low solubility of Ag_2S (Zhang, Xiao, and Fang, 2018; Devi et al., 2015; Opršal et al., 2021), the transformation of Ag_2S-NPs with potential release of Ag^+ and *in situ* formation of Ag_0 and Ag_0/Ag_2S-NPs hetero-nanostructures may possibly increase the toxicity (He et al., 2019). The reduced toxicity may also stem from intracellular Ag_2S formation sequestering free Ag^+ ions, thereby mitigating harmful effects such as inflammation (Gonzalez-Carter et al., 2017). Other EDX studies, performed in more complex intestinal *in vitro* models, also revealed colocalisation of silver with sulphur and phosphorus originating from endogenous regions, which may contain proteins (Lichtenstein et al., 2017a; Lichtenstein et al., 2017b; Georgantzopoulou et al., 2016). Additionally, Ag_2S formation at the particle surface was demonstrated in endosomal vesicles in mice microglia (Gonzalez-Carter et al., 2017), aligning with transformed E174-AgNPs observed in our study.

Altogether, these findings indicate that in addition to particle size, shape, and agglomeration state, physicochemical speciation (Kose et al., 2023) of E174-AgNPs, whether altered by transformations or not, may influence the cellular fate of the particles. It should be noted that while our study identified such transformations qualitatively, we did not perform quantitative analysis or distinguish between the ionic and particulate forms of Ag, and potential preparation artefacts cannot be excluded. However, we were able to observe that the uptake of E174-AgNPs (128.7 μg/mL) was associated with pronounced cellular alterations in Caco-2 cells, with the mitochondrial effects being the most notable, as evidenced by extensive mitochondrial swelling, damaged cristae, fluctuations in mitochondrial footprints and network morphology, and changes in the transcription of proteins related to proper mitochondrial function.

Cellular disturbances such as oxidative stress can lead to excessive

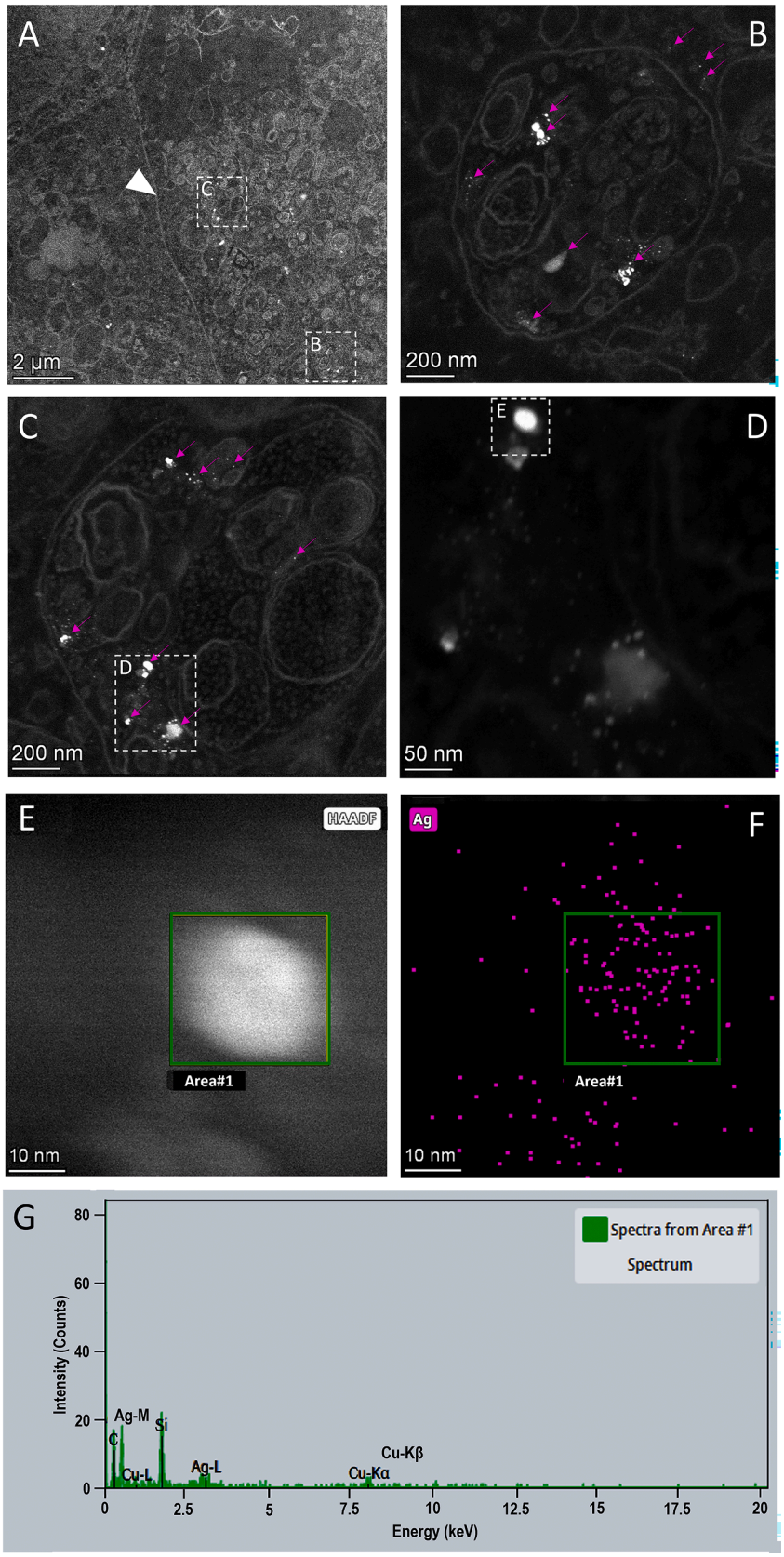

Fig. 5. Identification of E174-AgNPs in ultra-thin sections of Caco-2 cells after 24 h exposure to 128.7 µg/mL of E174-AgNPs. The HAADF-STEM micrograph (**A**) at low magnification (8kx) shows an overview of the cytoplasm of two adjacent Caco-2 cells containing E174-AgNPs (the white arrowhead indicates the cell membrane of an adjacent cell). Higher magnification micrographs (**B-C** = 62kx, **D** = 250kx, **E** = 1000kx) each show an enlarged image of the endo-/autolysosomes, indicated by dashed boxes. Pink arrows indicate E174-AgNPs in the endo-/autolysosomes (**B-C**), and the cytoplasm (**B**). The EDX spectral images correspond to Area#1 in the STEM micrograph E and represent Ag (**F**) and the complete spectrum (**G**).

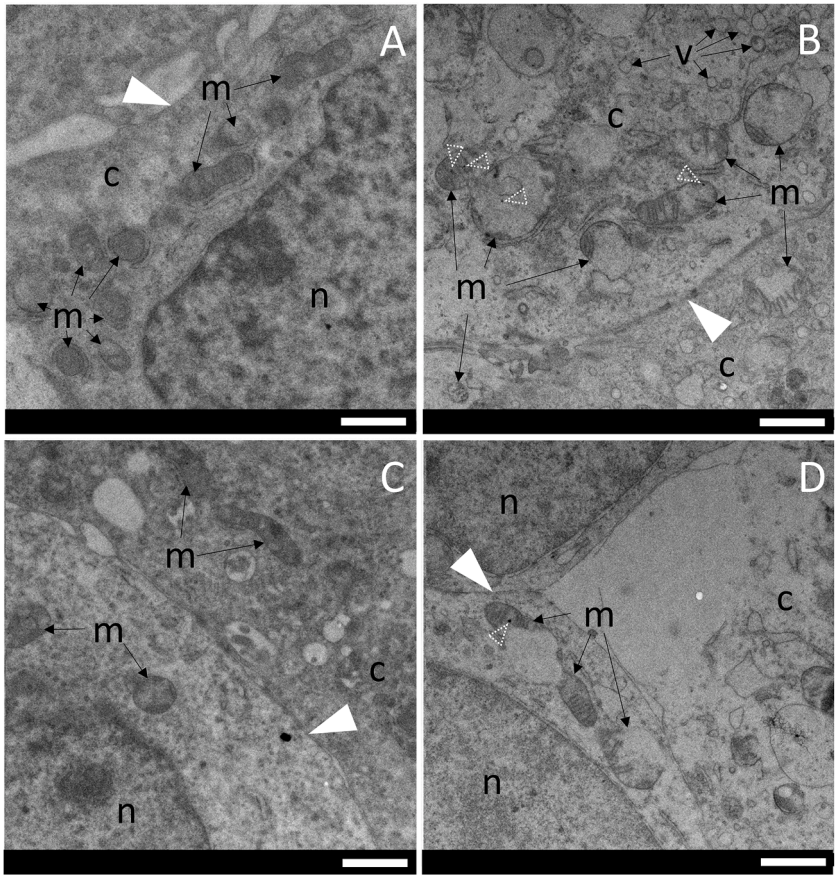

Fig. 6. Ultrastructural alterations induced by E174-AgNPs (128.7 µg/mL) after 24 h exposure. Representative micrographs of Caco-2 cells exposed to E174-AgNPs (**B** and **D**) are compared with control cells (**A** and **C**). E174-AgNPs-treated cells showed swollen mitochondria (**B**), electron-dense calcium-phosphate precipitates (**B** and **D**), and a highly vacuolated and electron-lucent cytoplasm (**B** and **D**). c – cytoplasm, n – nucleus, m – mitochondrion, v - vesicle, white arrowhead - cell membrane, dotted open arrowhead - $Ca_3(PO4)_2$ precipitates. Scale bar = 1 µm.

mitochondrial matrix swelling (Javadov, Chapa-Dubocq, and Makarov, 2018), but no increases in H_2O_2 were observed. However, the strong induction of *HMOX1* across all exposure conditions suggests increased oxidative stress levels from the first hours of exposure (5 h). Pathological mitochondrial swelling induces structural remodelling, which can lead to mitophagy-dependent removal of damaged mitochondria, rupture of the outer mitochondrial membrane (often triggering apoptosis), and/or dysregulated fusion and fission dynamics (Zhou et al., 2020). Mitophagy, or apoptosis, was demonstrated via the mitochondrial network morphology assessment through the presence of fragmented mitochondria that appeared smaller and less interconnected following 5 h exposure to E174-AgNPs. Similarly, PVP-AgNP exposure induced a significant reduction in network branching, indicating a comparable trend. Although less interconnected, the total cellular area occupied by the mitochondria was increased for most exposure conditions at this time point.

In contrast, after 24 h of exposure, cells exhibited increased mitochondrial branch length and network complexity, which was most pronounced at lower concentrations. This shift toward mitochondrial fusion is often associated with cell survival mechanisms, supporting increased mitochondrial ATP production to meet the cells' metabolic needs while facilitating the recycling of other biological materials (Rambold et al., 2011; Wai and Langer, 2016). In some conditions, these structural increases coincided with a reduction in mitochondrial footprint and mtDNAc, possibly reflecting the selective removal of damaged mitochondria. Such precipitates can form when excessive mitochondrial Ca^{2+} uptake exceeds buffering capacity, leading to the complexation of calcium with inorganic phosphate within the matrix. Similar mitochondrial calcium–phosphate formations have been described in association with calciprotein particles, where mitochondrial Ca^{2+} overload resulted in loss of membrane potential, impaired respiration, reduced mtDNAc, altered mitochondrial network morphology, and progressive mitochondrial elimination (Feenstra et al., 2025). Together, the presence of these calcium phosphate structures, the reduced mtDNA content, and the altered network organisation suggest that prolonged exposure to E174-AgNPs may disturb calcium homeostasis and promote mitochondrial calcium dysregulation, contributing to the selective removal of damaged mitochondria, potentially via mitophagy, while the remaining organelles undergo fusion to maintain cellular energy demands. The results of Zhou et al., (2020) support this hypothesis, as they also showed that mitochondrial topology transformations under stress conditions, such as swelling, lead to selective elimination by mitophagy (Zhou, Long, et al., 2020). It is known that in response to certain stressors, mitochondrial fragmentation can occur rapidly but is reversible once the stress is alleviated (Singh et al., 2025). Restoration of the mitochondrial membrane potential reactivates the fusion machinery, enabling the reconstruction of elongated, interconnected networks from smaller fragments (Singh et al., 2025). This regenerative process may be associated with the protective effects of particle sulfidation, though this relationship requires further investigation. Altogether, our results show that mitochondrial plasticity allows cells to adapt to changing environmental conditions and energy demands. Both E174-derived and PVP-AgNPs induced similar trends in mitochondrial alteration, though with notable differences. These disparities may arise from the smaller average size of PVP-AgNPs compared to E174-AgNPs, which, at the same concentration, results in a higher particle number. Additionally,

the PVP coating could influence particle stability and cellular interactions (Chen et al., 2016), potentially altering their bioavailability and impact on mitochondrial structure.

Both types of particles also exhibited comparable underlying gene expression profiles. The increased gene expression of heme oxygenase-1 (*HMOX1*) in our study suggests a cellular reaction to maintain mitochondrial health and functioning in all conditions (Consoli et al., 2021). Its induction via the NRF2/HMOX1 pathway upon cellular stressors contributes to mitochondrial protection, biogenesis, mitophagy, and overall cellular resilience (Chiang, Chen, and Chang, 2021; Dinkova-Kostova and Abramov, 2015). In response to oxidative stress, including elevated levels of H_2O_2, cellular signalling pathways that lead to the upregulation of HMOX1 as part of the cell's adaptive response are triggered (Chiang, Chen, and Chang, 2021). However, we did not find elevated levels of H_2O_2 after 24 h exposure of E174-AgNPs, suggesting that the activation of the signalling pathway likely occurred earlier in the timeframe, as suggested by the increased *HMOX1* expression after 5 h exposure. This is supported by the decreasing trends in the expression of other NRF2-ARE-regulated genes, such as *GSTP1* and *SOD2,* along with the differential expression patterns in other redox-related genes, *NOX1, CAT, GPX1,* and *ATOX1*, which only occurred significantly after 24 h exposure. The iron-transporter gene, *SLC11A2,* also showed decreased expression under these conditions. Zhai X et al. (2024) showed that AgNPs induce, along with differential expression of NRF2/HO-1 signalling pathway elements and cellular lipid peroxidation-dependent ferroptotic cell death, iron overload via iron transport disruption and ferritinophagy in mice (Zhai et al., 2024). Our findings, including increased membrane damage and mitochondrial/gene expression alterations, suggest the NRF2/HMOX1 pathway is a key defence mechanism against AgNP-induced cellular stress in intestinal cells. Consistent with other research (Aueviriyavit, Phummiratch, and Maniratanachote, 2014), this pathway acts as a stress sensor, activating HMOX1 to restore redox homeostasis and promote cell survival. We observed decreased mitochondrial DNA content, indicating disrupted mitochondrial integrity, and support the hypothesis that mitophagy may occur at high AgNP exposure (Gurunathan et al., 2018; Lee et al., 2014; Porter et al., 2021). HMOX1′s role as a hub gene in stress, apoptosis, and redox regulation, as seen in our and other studies (Porter et al., 2021; Bouwmeester et al., 2011; van der Zande et al., 2016), highlights its early response in cell survival. Nevertheless, because our study included only two exposure durations (5 h and 24 h), we cannot fully resolve the sequence of redox events. A more detailed time-resolved analysis would be required to clarify early *versus* late responses and to capture the dynamics of specific reactive oxygen species (ROS).

The results of the present study should be interpreted in light of several design considerations. First, the Caco-2 cell line was used as a proxy for the human intestinal epithelium. Although this model allows assessment of the direct cytotoxic effects of AgNPs, it does not fully replicate the structural complexity, barrier characteristics, or absorptive properties of mature enterocytes *in vivo*. Nevertheless, the Caco-2 model is widely used, facilitating comparison with existing literature generated under similar *in vitro* conditions. Second, the concentrations of E174-AgNPs were selected based on previously reported biological effects in non-food AgNPs rather than on realistic dietary exposure levels, and only a small fraction of ingested AgNPs is expected to reach the colon *in vivo*. However, the observed effects provide mechanistic insight that can be compared with existing *in vitro* toxicity studies on non-food AgNPs, thereby supporting the broader relevance of the AgNP literature to food-related particles, while acknowledging that material-specific characteristics and exposure conditions may influence outcomes *in vivo*. Finally, because the literature on particle-related effects is not always consistent, variability among studies may arise from differences in physicochemical properties, cell type, exposure duration, and concentration, all of which should be carefully considered and systematically assessed in future studies when interpreting and comparing findings. In addition, protein corona formation, which was not investigated in the present study, may provide valuable mechanistic insight into particle–cell interactions and resulting biological responses.

5. Conclusion

This study integrated the uptake, localisation, and physicochemical transformation of E174-AgNPs with subsequent intracellular ultrastructural changes and the induction of toxicity pathways in Caco-2 cells. Key findings were the comparable cytotoxic effects of E174-AgNPs and PVP-AgNPs in a concentration- and time-dependent manner, with the most pronounced toxicity observed following 24 h exposure. The observed cytotoxic effects were confirmed by a consistent induction of *HMOX1* expression in all exposure conditions, highlighting the involvement of oxidative stress and underscoring the role of mitochondrial dynamics, as evidenced by accompanying changes in mitochondrial network morphology. The qualitative physicochemical assessment after 24 h exposure to E174-AgNPs indicated a cascade of interconnected events leading to mitochondrial stress. More specifically, a combined effect of modified E174-AgNPs in endo-/autolysosomes and Ag-containing particles of a few nm in size near these endo-/autolysosomes culminated in mitochondrial swelling and rupture. In parallel, enhanced mitochondrial networking suggested a compensatory response by surviving mitochondria. These results set the base for a comprehensive understanding of the safety of E174-AgNPs in an *in vitro* intestinal model, and will contribute to the (re-)evaluation of the hazard and risk assessment of the food additive E174.

Ethics approval

Not applicable.

Consent for publication

Not applicable.

Availability of data and materials

The datasets supporting the conclusions of this article can be retrieved from the corresponding author upon reasonable request.

Disclosure statement

The authors report there are no competing interests to declare.

Funding

This research was supported by the [BOF UHasselt] under Grant [R9782]; [FWO] under Grant [G.0B83.17N]; [FWO] under Grant [1258725N] assigned to N.D.S; and [EMBRC Belgium] under [GOH3817N].

CRediT authorship contribution statement

ND Saenen: Writing – original draft, Visualization, Methodology, Investigation, Formal analysis, Conceptualization. **S De Vos:** Writing – original draft, Visualization, Methodology, Investigation, Formal analysis. **E Verleysen:** Writing – review & editing, Resources, Methodology, Investigation. **MS Witters:** Writing – review & editing, Methodology, Investigation, Formal analysis. **F Van Belleghem:** Writing – review & editing, Investigation, Formal analysis. **J Mast:** Writing – review & editing, Supervision, Resources, Conceptualization. **K Smeets:** Writing – review & editing, Supervision, Resources, Funding acquisition.

Declaration of competing interest

The authors declare that they have no known competing financial interests or personal relationships that could have appeared to influence the work reported in this paper.

Acknowledgements

The authors kindly thank Natascha Steffanie and Ria Vanderspikken for their dependable technical assistance, and the IMO-MAF-NSI-Nanobiophysics and soft matter interfaces group for the use of their DLS infrastructure.

Supplementary materials

Supplementary material associated with this article can be found, in the online version, at doi:10.1016/j.hazadv.2026.101247.

References

Akter, M., Sikder, M.T., Rahman, M.M., Ullah, A.K.M.A., Hossain, K.F.B., Banik, S., Hosokawa, T., Saito, T., Kurasaki, M., 2018. A systematic review on silver nanoparticles-induced cytotoxicity: physicochemical properties and perspectives. J. Adv. Res. 9, 1–16. https://doi.org/10.1016/j.jare.2017.10.008.

AshaRani, P.V., Low Kah Mun, G., Prakash Hande, M., Valiyaveettil, S., 2009. Cytotoxicity and genotoxicity of silver nanoparticles in Human cells. ACS. Nano 3 (2), 279–290. https://doi.org/10.1021/nn800596w.

Aueviriyavit, S., Phummiratch, D., Maniratanachote, R., 2014. Mechanistic study on the biological effects of silver and gold nanoparticles in Caco-2 cells–induction of the Nrf2/HO-1 pathway by high concentrations of silver nanoparticles. Toxicol. Lett. 224 (1), 73–83. https://doi.org/10.1016/j.toxlet.2013.09.020.

European Food Safety Authority, 2016. Scientific opinion on the re-evaluation of silver (E 174) as food additive. EFSA J. 14 (1), 4364. https://doi.org/10.2903/j.efsa.2016.4364.

European Food Safety Authority, 2025. Follow-up of the re-evaluation of silver (E 174) as a food additive (EFSA-Q-2023-00169). EFSA J. 23 (4), e9316. https://doi.org/10.2903/j.efsa.2025.9316.

Bobyk, L., Tarantini, A., Béal, D., Veronesi, G., Kieffer, I., Motellier, S., Valsami-Jones, E., Lynch, I., Jouneau, P., Pernet-Gallay, K., Aude-Garcia, C., Sauvaigo, S., Douki, T., Rabilloud, T., Carriere, M., 2021. Toxicity and chemical transformation of silver nanoparticles in A549 lung cells: dose-rate-dependent genotoxic impact. Environ. Sci.: Nano 8, 806–821. https://doi.org/10.1039/D0EN00533A.

Bouwmeester, H., Poortman, J., Peters, R.J., Wijma, E., Kramer, E., Makama, S., Puspitaninganindita, K., Marvin, H.J., Peijnenburg, A.A., Hendriksen, P.J., 2011. Characterization of translocation of silver nanoparticles and effects on whole-genome gene expression using an in vitro intestinal epithelium coculture model. ACS. Nano 5 (5), 4091–4103. https://doi.org/10.1021/nn2007145.

Brandon, E.F., Bosch, T.M., Deenen, M.J., Levink, R., van der Wal, E., van Meerveld, J.B., Bijl, M., Beijnen, J.H., Schellens, J.H., Meijerman, I., 2006. Validation of in vitro cell models used in drug metabolism and transport studies; genotyping of cytochrome P450, phase II enzymes and drug transporter polymorphisms in the human hepatoma (HepG2), ovarian carcinoma (IGROV-1) and colon carcinoma (CaCo-2, LS180) cell lines. Toxicol. Appl. Pharmacol. 211 (1), 1–10. https://doi.org/10.1016/j.taap.2005.05.004.

Bustin, S.A., Benes, V., Garson, J.A., Hellemans, J., Huggett, J., Kubista, M., Mueller, R., Nolan, T., Pfaffl, M.W., Shipley, G.L., Vandesompele, J., Wittwer, C.T., 2009. The MIQE guidelines: minimum information for publication of quantitative real-time PCR experiments. Clin. Chem. 55 (4), 611–622. https://doi.org/10.1373/clinchem.2008.112797.

Chen, N., Song, Z.-M., Tang, H., Xi, W.-S., Cao, A., Liu, Y., Wang, H., 2016. Toxicological effects of caco-2 cells following short-term and long-term exposure to Ag nanoparticles. Int. J. Mol. Sci. 17, 974. https://doi.org/10.3390/ijms17060974.

Chiang, S.K., Chen, S.E., Chang, L.C., 2021. The role of HO-1 and its crosstalk with oxidative stress in cancer cell survival. Cells 10 (9), 2401. https://doi.org/10.3390/cells10092401.

Consoli, V., Sorrenti, V., Grosso, S., Vanella, L., 2021. Heme oxygenase-1 signaling and redox homeostasis in physiopathological conditions. Biomolecules 11 (4), 589. https://doi.org/10.3390/biom11040589.

Dąbrowska-Bouta, B., Sulkowski, G., Strużyński, W., Strużyńska, L., 2019. Prolonged exposure to silver nanoparticles results in oxidative stress in cerebral myelin. Neurotox. Res. 35, 495–504. https://doi.org/10.1007/s12640-018-9977-0.

de la Calle, I., Menta, M., Klein, M., Séby, F., 2018. Study of the presence of micro- and nanoparticles in drinks and foods by multiple analytical techniques. Food Chem. 266, 133–145. https://doi.org/10.1016/j.foodchem.2018.05.107.

De Matteis, V., 2017. Exposure to inorganic nanoparticles: routes of entry, immune response, biodistribution and In vitro/In vivo toxicity evaluation. Toxics 5 (4), 29. https://doi.org/10.3390/toxics5040029.

De Vos, S., Waegeneers, N., Verleysen, E., Smeets, K., Mast, J., 2020. Physico-chemical characterisation of the fraction of silver (nano)particles in pristine food additive E174 and in E174-containing confectionery. Food Addit. Contam. Part a Chem. Anal. Control Expo Risk. Assess. 37 (11), 1831–1846. https://doi.org/10.1080/19440049.2020.1809719.

Devi, G.P., Ahmed, K.B., Varsha, M.K., Shrijha, B.S., Lal, K.K., Anbazhagan, V., Thiagarajan, R., 2015. Sulfidation of silver nanoparticle reduces its toxicity in zebrafish. Aquat. Toxicol. 158, 149–156. https://doi.org/10.1016/j.aquatox.2014.11.007.

Dinkova-Kostova, A.T., Abramov, A.Y., 2015. The emerging role of Nrf2 in mitochondrial function. Free Radic. Biol. Med. 88, 179–188. https://doi.org/10.1016/j.freeradbiomed.2015.04.036. Part B.

European Chemical Agency (ECHA), 2022. Appendix for nanoforms applicable to the Guidance on registration and substance identification, Version 2.0. Helsinki: European Chemical Agency. Available at: https://echa.europa.eu/documents/10162/17250/how_to_register_nano_en.pdf/f8c046ec-f60b-4349-492b-e915fd9e3ca0.

European Parliament, Council of the European Union, 2010. Directive 2010/63/EU of 22 September 2010 on the protection of animals used for scientific purpose Text with EEA relevance. Official Journal of the European Union. Available at: http://data.europa.eu/eli/dir/2010/63/oj.

Feenstra, L., Zeper, L.W., van de Langenberg, B., Kahlman, E.J.E.M., de La Roij, G., Reijrink, M., Bernay, B., Chatre, L., Kuipers, J., Giepmans, B.N.G., Mastik, M.F., Kooistra, W., Lodewijk, M.E., Zuidscherwoude, M., Smith, E.R., Krenning, G., de Baaij, J.H.F., Hillebrands, J.L., Hoenderop, J.G.J., 2025. Calciprotein particle-activated endothelial cells aggravate smooth muscle cell calcification via paracrine signalling. Cell Mol. Life Sci. 82 (1), 177. https://doi.org/10.1007/s00018-025-05702-z.

Ferdous, Z., Nemmar, A., 2020. Health impact of silver nanoparticles: a review of the biodistribution and toxicity following various routes of exposure. Int. J. Mol. Sci. 21 (7), 2375. https://doi.org/10.3390/ijms21072375.

Ferreira, L.A.B., dos Reis, S.B., Nascimento da Silva, E., Cadore, S., Bernardes, J.D.S., Durán, N., de Jesus, M.B., 2020. Thiol-antioxidants interfere with assessing silver nanoparticle cytotoxicity. Nanomedicine 24, 102130. https://doi.org/10.1016/j.nano.2019.102130.

Gan, J., Sun, J., Chang, X., Li, W., Li, J., Niu, S., Kong, L., Zhang, T., Wu, T., Tang, M., Xue, Y., 2020. Biodistribution and organ oxidative damage following 28 days oral administration of nanosilver with/without coating in mice. J. Appl. Toxicol. 40 (6), 815–831. https://doi.org/10.1002/jat.3946.

García-Rodríguez, A., Vila, L., Cortés, C., Hernández, A., Marcos, R., 2018. Exploring the usefulness of the complex in vitro intestinal epithelial model Caco-2/HT29/Raji-B in nanotoxicology. Food Chem. Toxicol. 113, 162–170. https://doi.org/10.1016/j.fct.2018.01.042.

Georgantzopoulou, A., Cambier, S., Serchi, T., Kruszewski, M., Balachandran, Y.L., Grysan, P., Audinot, J.N., Ziebel, J., Guignard, C., Gutleb, A.C., Murk, A.J., 2016. Inhibition of multixenobiotic resistance transporters (MXR) by silver nanoparticles and ions in vitro and in Daphnia magna. Sci. Total. Environ. 569-570, 681–689. https://doi.org/10.1016/j.scitotenv.2016.06.157.

Gerloff, K., Albrecht, C., Boots, A., Förster, I., Schins, R., 2009. Cytotoxicity and oxidative DNA damage by nanoparticles in human intestinal Caco-2 cells. Nanotoxicology 3 (4), 355–364. https://doi.org/10.3109/17435390903276933.

Gonzalez-Carter, D.A., Leo, B.F., Ruenraroengsak, P., Chen, S., Goode, A.E., Theodorou, I.G., Chung, K.F., Carzaniga, R., Shaffer, M.S., Dexter, D.T., Ryan, M.P., Porter, A.E., 2017. Silver nanoparticles reduce brain inflammation and related neurotoxicity through induction of H(2)S-synthesizing enzymes. Sci. Rep. 7, 42871. https://doi.org/10.1038/srep42871.

Gurunathan, S., Qasim, M., Park, C., Yoo, H., Choi, D.Y., Song, H., Park, C., Kim, J.H., Hong, K., 2018. Cytotoxicity and transcriptomic analysis of silver nanoparticles in mouse embryonic fibroblast cells. Int. J. Mol. Sci. 19 (11), 3618. https://doi.org/10.3390/ijms19113618.

He, D., Garg, S., Wang, Z., Li, L., Rong, H., Ma, X., Li, G., An, T., Waite, T.D., 2019. Silver sulfide nanoparticles in aqueous environments: formation, transformation and toxicity. Environ. Sci.: Nano 6, 1674–1687. https://doi.org/10.1039/C9EN00138G.

Javadov, S., Chapa-Dubocq, X., Makarov, V., 2018. Different approaches to modeling analysis of mitochondrial swelling. Mitochondrion 38, 58–70. https://doi.org/10.1016/j.mito.2017.08.004.

Kose, O., Béal, D., Motellier, S., Pelissier, N., Collin-Faure, V., Blosi, M., Bengalli, R., Costa, A., Furxhi, I., Mantecca, P., Carriere, M., 2023. Physicochemical transformations of silver nanoparticles in the oro-gastrointestinal tract mildly affect their toxicity to intestinal cells In vitro: an AOP-oriented testing approach. Toxics 11 (3), 199. https://doi.org/10.3390/toxics11030199.

Lee, Y.H., Cheng, F.Y., Chiu, H.W., Tsai, J.C., Fang, C.Y., Chen, C.W., Wang, Y.J., 2014. Cytotoxicity, oxidative stress, apoptosis and the autophagic effects of silver nanoparticles in mouse embryonic fibroblasts. Biomaterials 35 (16), 4706–4715. https://doi.org/10.1016/j.biomaterials.2014.02.021.

Lefebvre, D.E., Venema, K., Gombau, L., Valerio Jr., L.G., Raju, J., Bondy, G.S., Bouwmeester, H., Singh, R.P., Clippinger, A.J., Collnot, E.M., Mehta, R., Stone, V., 2015. Utility of models of the gastrointestinal tract for assessment of the digestion and absorption of engineered nanomaterials released from food matrices. Nanotoxicology 9 (4), 523–542. https://doi.org/10.3109/17435390.2014.948091.

Liao, C., Li, Y., Tjong, S.C., 2019. Bactericidal and cytotoxic properties of silver nanoparticles. Int. J. Mol. Sci. 20 (2), 449. https://doi.org/10.3390/ijms20020449.

Lichtenstein, D., Ebmeyer, J., Meyer, T., Behr, A.C., Kästner, C., Böhmert, L., Juling, S., Niemann, B., Fahrenson, C., Selve, S., Thünemann, A.F., Meijer, J., Estrela-Lopis, I., Braeuning, A., Lampen, A., 2017a. It takes more than a coating to get nanoparticles through the intestinal barrier in vitro. Eur. J. Pharm. Biopharm. 118, 21–29. https://doi.org/10.1016/j.ejpb.2016.12.004.

Lichtenstein, D., Meyer, T., Böhmert, L., Juling, S., Fahrenson, C., Selve, S., Thünemann, A., Meijer, J., Estrela-Lopis, I., Braeuning, A., Lampen, A., 2017b.

Dosimetric quantification of coating-related uptake of silver nanoparticles. Langmuir 33 (45), 13087–13097. https://doi.org/10.1021/acs.langmuir.7b01851.
Liu, J., Wang, Z., Liu, F.D., Kane, A.B., Hurt, R.H., 2012. Chemical transformations of nanosilver in biological environments. ACS. Nano 6 (11), 9887–9899. https://doi.org/10.1021/nn303449n.
Loza, K., Sengstock, C., Chernousova, S., Köller, M., Epple, M., 2014. The predominant species of ionic silver in biological media is colloidally dispersed nanoparticulate silver chloride. RSC. Adv. 4, 35290. https://doi.org/10.1039/C4RA04764H.
Marchioni, M., Jouneau, P.H., Chevallet, M., Michaud-Soret, I., Deniaud, A., 2018. Silver nanoparticle fate in mammals: bridging in vitro and in vivo studies. Coord. Chem. Rev. 364, 118–136. https://doi.org/10.1016/j.ccr.2018.03.008.
Martirosyan, A., Grintzalis, K., Polet, M., Laloux, L., Schneider, Y.J., 2016. Tuning the inflammatory response to silver nanoparticles via quercetin in Caco-2 (co-)cultures as model of the human intestinal mucosa. Toxicol. Lett. 253, 36–45. https://doi.org/10.1016/j.toxlet.2016.04.018.
Maurer, L.L., Meyer, J.N., 2016. A systematic review of evidence for silver nanoparticle-induced mitochondrial toxicity. Environ. Sci.: Nano 3, 311–322. https://doi.org/10.1039/C5EN00187K.
Medina-Reyes, E.I., Rodríguez-Ibarra, C., Déciga-Alcaraz, A., Díaz-Urbina, D., Chirino, Y. I., Pedraza-Chaverri, J., 2020. Food additives containing nanoparticles induce gastrotoxicity, hepatotoxicity and alterations in animal behavior: the unknown role of oxidative stress. Food Chem. Toxicol. 146, 111814. https://doi.org/10.1016/j.fct.2020.111814.
Miethling-Graff, R., Rumpker, R., Richter, M., Verano-Braga, T., Kjeldsen, F., Brewer, J., Hoyland, J., Rubahn, H.G., Erdmann, H., 2014. Exposure to silver nanoparticles induces size- and dose-dependent oxidative stress and cytotoxicity in human colon carcinoma cells. Toxicol. In. Vitro 28 (7), 1280–1289. https://doi.org/10.1016/j.tiv.2014.06.005.
Molleman, B., Hiemstra, T., 2015. Surface structure of silver nanoparticles as a model for understanding the oxidative dissolution of silver ions. Langmuir 31 (49), 13361–13372. https://doi.org/10.1021/acs.langmuir.5b03686.
Opršal, J., Knotek, P., Zickler, G.A., Sigg, L., Schirmer, K., Pouzar, M.;., Geppert, M.C., 2021. Accumulation and translocation of silver and silver sulfide nanoparticles in contact with Rainbow trout intestinal cells. Aquat. Toxicol. 237, 105869. https://doi.org/10.1016/j.aquatox.2021.105869.
Panzarini, E., Mariano, S., Carata, E., Mura, F., Rossi, M., Dini, L., 2018. Intracellular transport of silver and gold nanoparticles and biological responses: an update. Int. J. Mol. Sci. 19 (5), 1305. https://doi.org/10.3390/ijms19051305.
Persaud, I., Shannahan, J.H., Raghavendra, A.J., Alsaleh, N.B., Podila, R., Brown, J.M., 2019. Biocorona formation contributes to silver nanoparticle induced endoplasmic reticulum stress. Ecotoxicol. Environ. Saf. 170, 77–86. https://doi.org/10.1016/j.ecoenv.2018.11.107.
Polet, M., Laloux, L., Cambier, S., Ziebel, J., Gutleb, A.C., Schneider, Y.J., 2020. Soluble silver ions from silver nanoparticles induce a polarised secretion of interleukin-8 in differentiated Caco-2 cells. Toxicol. Lett. 325, 14–24. https://doi.org/10.1016/j.toxlet.2020.02.004.
Porter, G.C., Duncan, W.J., Jude, A., Abdelmoneim, D., Easingwood, R.A., Coates, D.E., 2021. Endocytosed silver nanoparticles degrade in lysosomes to form secondary nanoparticle structures during expression of autophagy genes in osteogenic cells. Nanomedicine 33, 102355. https://doi.org/10.1016/j.nano.2020.102355.
Powell, J.J., Faria, N., Thomas-McKay, E., Pele, L.C., 2010. Origin and fate of dietary nanoparticles and microparticles in the gastrointestinal tract. J. Autoimmun. 34 (3), J226–J233. https://doi.org/10.1016/j.jaut.2009.11.006.
Rambold, A.S., Kostelecky, B., Elia, N., Lippincott-Schwartz, J., 2011. Tubular network formation protects mitochondria from autophagosomal degradation during nutrient starvation. Proc. Natl. Acad. Sci. USA 108 (25), 10190–10195. https://doi.org/10.1073/pnas.1107402108.
Saenen, N.D., Witters, M.S., Hantoro, I., Tejeda, I., Ethirajan, A., Van Belleghem, F., Smeets, K., 2023. Polystyrene microplastics of varying sizes and shapes induce distinct redox and mitochondrial stress responses in a Caco-2 monolayer. Antioxid. (Basel) 12 (3), 739. https://doi.org/10.3390/antiox12030739.
Singh, G., Vengayil, V., Khanna, A., Adhikary, S., Laxman, S., 2025. Active control of mitochondrial network morphology by metabolism-driven redox state. Proc. Natl. Acad. Sci. USA 122 (16), e2421953122. https://doi.org/10.1073/pnas.2421953122.
Song, Y., Guan, R., Lyu, F., Kang, T., Wu, Y., Chen, X., 2014. In vitro cytotoxicity of silver nanoparticles and zinc oxide nanoparticles to human epithelial colorectal adenocarcinoma (Caco-2) cells. Mutat. Res. 769, 113–118. https://doi.org/10.1016/j.mrfmmm.2014.08.001.
Taboada-López, M.V., Leal-Martínez, B.H., Domínguez-González, R., Bermejo-Barrera, P., Taboada-Antelo, P., Moreda-Piñeiro, A., 2021. Caco-2 in vitro model of human gastrointestinal tract for studying the absorption of titanium dioxide and silver nanoparticles from seafood. Talanta 233, 122494. https://doi.org/10.1016/j.talanta.2021.122494.
Valente, A.J., Maddalena, L.A., Robb, E.L., Moradi, F., Stuart, J.A., 2017. A simple ImageJ macro tool for analysing mitochondrial network morphology in mammalian cell culture. Acta Histochem. 119, 315–326. https://doi.org/10.1016/j.acthis.2017.03.001.
van der Zande, M., Undas, A.K., Kramer, E., Monopoli, M.P., Peters, R.J., Garry, D., Antunes Fernandes, E.C., Hendriksen, P.J., Marvin, H.J., Peijnenburg, A.A., Bouwmeester, H., 2016. Different responses of Caco-2 and MCF-7 cells to silver nanoparticles are based on highly similar mechanisms of action. Nanotoxicology 10 (10), 1431–1441. https://doi.org/10.1080/17435390.2016.1225132.
Verleysen, E., Van Doren, E., Waegeneers, N., De Temmerman, P.J., Abi Daoud Francisco, M., Mast, J., 2015. TEM and SP-ICP-MS analysis of the release of silver nanoparticles from decoration of pastry. J. Agric. Food Chem. 63 (13), 3570–3578. https://doi.org/10.1021/acs.jafc.5b00578.
Verleysen, E., Wagner, T., Lipinski, H.G., Kagi, R., Koeber, R., Boix-Sanfeliu, A., De Temmerman, P.J., Mast, J., 2019. Evaluation of a TEM based approach for size measurement of particulate (Nano)materials. Mater. (Basel) 12 (14), 2274. https://doi.org/10.3390/ma12142274.
Wagner, T., Eglinger, E.P., 2017. ParticleSizer plugin for ImageJ/Fiji. Accessed 08/03/2020. Available at: https://imagej.net/plugins/particlesizer.
Wai, T., Langer, T., 2016. Mitochondrial dynamics and metabolic regulation. Trends. Endocrinol. Metab. 27 (2), 105–117. https://doi.org/10.1016/j.tem.2015.12.001.
Wang, J., Che, B., Zhang, L.W., Dong, G., Luo, Q., Xin, L., 2017. Comparative genotoxicity of silver nanoparticles in human liver HepG2 and lung epithelial A549 cells. J. Appl. Toxicol. 37 (4), 495–501. https://doi.org/10.1002/jat.3385.
Wu, M., Guo, H., Liu, L., Liu, Y., Xie, L., 2019. Size-dependent cellular uptake and localisation profiles of silver nanoparticles. Int. J. Nanomed. 14, 4247–4259. https://doi.org/10.2147/IJN.S201107.
Xu, K., Basu, N., George, S., 2021. Dietary nanoparticles compromise epithelial integrity and enhance translocation and antigenicity of milk proteins: an in vitro investigation. NanoImpact 24, 100369. https://doi.org/10.1016/j.impact.2021.100369.
Zhai, X., Yan, W., Liu, S., Tian, L., Zhai, X., Yan, W., Liu, S., Tian, L., Zhang, Y., Zhao, Y., Ni, Y., Shen, H., Wang, J., Wan, Z., Jiang, F., Xin, L., 2024. Silver nanoparticles induce iron accumulation-associated cognitive impairment via modulating neuronal ferroptosis. Environ. Pollut. 346, 123555. https://doi.org/10.1016/j.envpol.2024.123555.
Zhang, X.F., Shen, W., Gurunathan, S., 2016. Silver nanoparticle-mediated cellular responses in various cell lines: an in vitro model. Int. J. Mol. Sci. 17 (10), 1603. https://doi.org/10.3390/ijms17101603.
Zhang, W., Xiao, B., Fang, T., 2018. Chemical transformation of silver nanoparticles in aquatic environments: mechanism, morphology and toxicity. Chemosphere 191, 324–334. https://doi.org/10.1016/j.chemosphere.2017.10.016.
Zhou, Y., Long, Q., Wu, H., Li, W., Qi, J., Wu, Y., Xiang, G., Tang, H., Yang, L., Chen, K., Li, L., Bao, F., Li, H., Wang, Y., Li, M., Liu, X., 2020. Topology-dependent, bifurcated mitochondrial quality control under starvation. Autophagy 16 (3), 562–574. https://doi.org/10.1080/15548627.2019.1634944.